# Diphtheria Toxin Catalyzed Hydrolysis of $NAD^+$: Molecular Dynamics Study of Enzyme-Bound Substrate, Transition State, and Inhibitor

**Kalju Kahn and Thomas C. Bruice***

*Contribution from the Department of Chemistry and Biochemistry, University of California, Santa Barbara, Santa Barbara, California 93106*

*Received June 5, 2001*

**Abstract:** The mechanism of the diphtheria toxin-catalyzed hydrolysis of $NAD^+$ was investigated by quantum chemical calculations and molecular dynamics simulations. Several effects that could explain the 6000-fold rate acceleration ($\Delta\Delta G^{\ddagger} \sim 5$ kcal/mol) by the enzyme were considered. First, the carboxamide arm of the enzyme-bound $NAD^+$ adopts a trans conformation while the most stable conformation is cis. The most stable conformation for the nicotinamide product has the amide carbonyl trans. The activation energy for the cleavage of the ribosidic bond is reduced by 2 kcal/mol due to the relaxation of this ground state conformational stress in the transition state. Second, molecular dynamics simulations to the nanosecond time range revealed that the carboxylate of Glu148 forms a hydrogen bond to the substrate's 2′ hydroxyl group in E·S (∼17% of the time) and E·TS (∼57% of the time) complexes. This interaction is not seen in crystal structures. The ApUp inhibitor is held more tightly by the enzyme than the transition state and the substrate. Analysis of correlated motions reveals differences in the pattern of anticorrelated motions for protein backbone atoms when the transition state occupies the active site as compared to the E·$NAD^+$ complex.

## Introduction

Diphtheria toxin (DT) is a 535 residue protein consisting of a catalytic domain (residues 1−193), a membrane-inserting domain (residues 205−378), and a receptor binding domain (residues 386−535).[1] The catalytic domain of diphtheria toxin (E.C. 2.4.2.36) has $NAD^+$:diphthamide ADP−ribosyltransferase activity (Scheme 1). The natural acceptor for the $NAD^+$ ribosyl moiety is the eucaryotic elongation factor 2 (EF2).[2] Ribosylation of a modified histidine residue in EF2 halts protein synthesis at ribosomes and results in cell death. It has been demonstrated that entry of a single catalytic domain of DT is sufficient for cell death.[3] In the absence of an acceptor molecule, the catalytic domain has slow $NAD^+$ hydrolase activity.

The structures of the whole diphtheria toxin as well as that of the catalytic subunit have been determined by X-ray crystallography.[4−6] The nature of the transition state for DT-catalyzed $NAD^+$ hydrolysis has been determined via measurement of multiple kinetic isotope effects.[7] These results indicate that the hydrolysis occurs via a concerted $A_ND_N$ nucleophilic displacement ($S_N2$) mechanism and involves a transition state resembling an exploded ribo-oxocarbenium ion. The kinetics of the ADP−ribosylation reaction as well as the enzyme-catalyzed $NAD^+$ hydrolysis have been studied with wild-type and mutant enzymes.[8−12] It should be noted that the crystallographic structure of the monomeric catalytic subunit with bound $NAD^+$ has not been determined. Thus details of binding of the substrate in the catalytically active enzyme are in doubt.

We have investigated the structure of DT bound to its substrate $NAD^+$, endogenous inhibitor ApUp, and two models for the transition state of the $NAD^+$−glycohydrolase reaction via molecular dynamic (MD) simulations. In addition, the conformational energies of the reactant and the leaving group have been estimated from ab initio calculations.

## Methods

**General Setup.** MD simulations of diphtheria toxin catalytic subunit were performed with the program CHARMM (version 25b2).[13] Complexes of the enzyme with its endogenous inhibitor adenylyl-(3′→5′)uridine 3′-monophosphate (ApUp, Chart 1), with the substrate

* To whom correspondence should be addressed. (phone) (805) 893-2044; (fax) (805) 893-2229; (e-mail) tcbruice@bioorganic.ucsb.edu.

(1) Eisenberg, D.; Bell, C. E.; Bennett, M. J.; Collier, R. J.; Schlunegger, M. P.; Steere, B. A.; Weiss, M. S. A Structure-Based Model of Diphtheria Toxin Action. In *Protein Toxin Structure*; Parker, M. W., Ed.; Landes: Austin, TX, 1996; pp 25−47.

(2) Honjo, T.; Nishizuka, Y.; Hayaishi, O.; Kato, I. *J. Biol. Chem.* **1968**, *243*, 3553−3555.

(3) Yamaizumi, M.; Mekada, E.; Uchida, T.; Okada, Y. *Cell* **1978**, *15*, 245−250.

(4) Choe, S.; Bennett, M. J.; Fujii, G.; Curmi, P. M. G.; Kantardjieff, K. A.; Collier, R. J.; Eisenberg, D. *Nature* **1992**, *357*, 216−222.

(5) Bell, C. E.; Eisenberg, D. *Biochemistry* **1996**, *35*, 1137−1149.

(6) Bell, C. E.; Eisenberg, D. *Biochemistry* **1997**, *36*, 481−488.

(7) Berti, P. J.; Blanke, S. R.; Schramm, V. L. *J. Am. Chem. Soc.* **1997**, *119*, 12079−12088.

(8) Papini, E.; Schiavo, G.; Rappuoli, R.; Montecucco, C. *Toxicon* **1990**, *28*, 631−635.

(9) Blanke, S. R.; Huang, K.; Wilson, B. A.; Papini, E.; Covacci, A.; Collier, R. J. *Biochemistry* **1994**, *33*, 5155−5161.

(10) Blanke, S. R.; Huang, K.; Collier, R. J. *Biochemistry* **1994**, *33*, 15494−15500.

(11) Wilson, B. A.; Reich, K. A.; Weinstein, B. R.; Collier, R. J. *Biochemistry* **1990**, *29*, 8643−8651.

(12) Wilson, B. A.; Blanke, S. R.; Reich, K. A.; Collier, R. J. *J. Biol. Chem.* **1994**, *269*, 23296−23301.

(13) Brooks, B. R.; Bruccoleri, R. E.; Olafson, B. D.; States, D. J.; Swaminathan, S.; Karplus, M. *J. Comput. Chem.* **1983**, *4*, 187−217.

10.1021/ja0113807 CCC: $20.00 
Published on Web 11/08/2001

**Scheme 1**

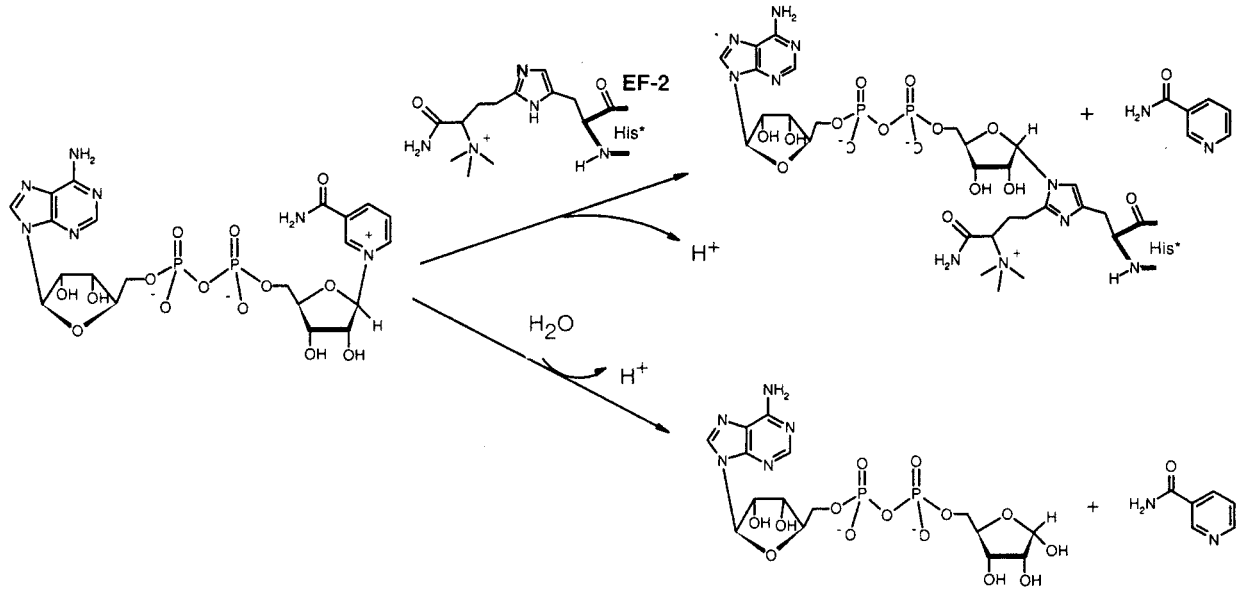


**Chart 1.** ApUp and Its Main Interactions with DT

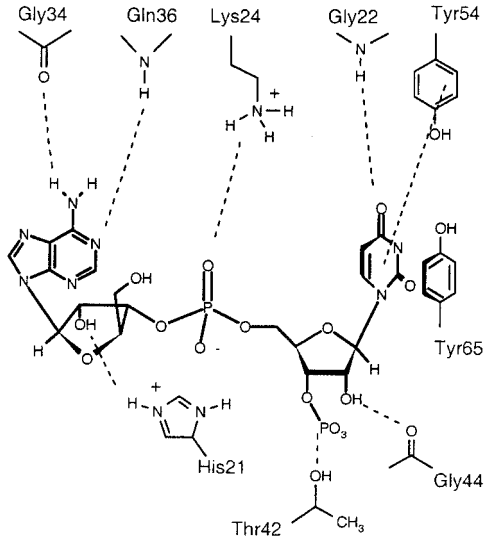


**Chart 2.** $NAD^+$ and Its Main Interactions with DT

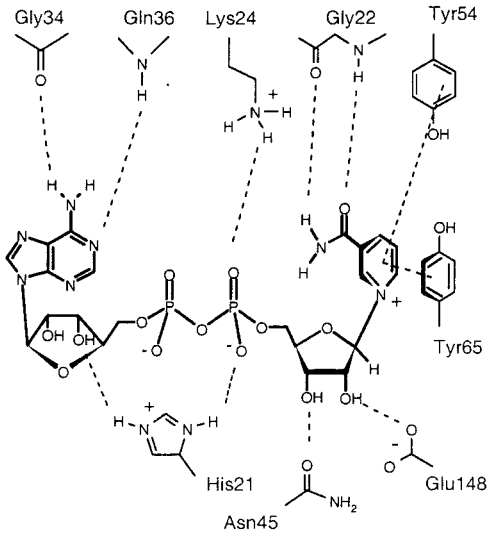


nicotinamide adenine dinucleotide ($NAD^+$, Chart 2), and with two models of transition state (TS) for the $NAD^+$ hydrolysis were studied. In the first model of the TS, the nucleophilic water molecule was part of the water pool and no explicit bond was defined between this water and the rest of the system. In the second TS simulation, the incoming water molecule was explicitly bonded to the C1′ of the ribosyl ring. These four simulations will be referred to as E·I, E·S, E·TS, and E·TS−$H_2O$, respectively, in the following discussion. For the E·I simulation, the initial coordinates for protein atoms as well as those of ApUp were taken from the crystal structure of the isolated catalytic domain of DT complexed with ApUp (1DTP).[14] The initial coordinates of the DT−$NAD^+$ complex were obtained by docking $NAD^+$ from the low-temperature structure of the dimeric diphtheria toxin with $NAD^+$ (1TOX)[5] into the structure 1DTP after overlaying the protein backbone atoms. Transition state models were docked to the active site for E·TS and E·TS−$H_2O$ simulations. The partial structure of TS was provided to us by Prof. Paul Berti.[7] We refined this model as described below to give the starting structure of the bound transition state.

**Force Field for the Transition State.** Standard CHARMM22 all-atom force field parameters were used for modeling ApUp and $NAD^+$.[15,16] There are no parameters in CHARMM for describing the transition state for $NAD^+$ hydrolysis. These parameters were estimated based on experimental KIE's and ab initio calculations with Gaussian98[17] as outlined in Chart 3. Our approach is very similar to that taken previously[18] except that we are using MP2/6-31+G(d,p) and MP2/aug-cc-pVTZ reference structures and smaller models versus HF/6-31(d,p) structures and more complete models. First, structures of models for reactants and products (Charts 4 and 5) were optimized at the MP2/

(14) Weiss, M. S.; Blanke, S. R.; Collier, R. J.; Eisenberg, D. *Biochemistry* **1995**, *34*, 773−781.

(15) MacKerell, A. D., Jr.; Wiórkiewicz-Kuczera, J.; Karplus, M. *J. Am. Chem. Soc.* **1995**, *117*, 11946−11975.

(16) Pavelites, J. J.; Gao, J. L.; Bash, P. A.; MacKerell, A. D., Jr. *J. Comput. Chem.* **1997**, *18*, 221−239.

(17) Frisch, M. J.; Trucks, G. W.; Schlegel, H. B.; Scuseria, G. E.; Robb, M. A.; Cheeseman, J. R.; Zakrzewski, V. G.; Montgomery, J. A. J.; Stratmann, R. E.; Burant, J. C.; Dapprich, S.; Millam, J. M.; Daniels, A. D.; Kudin, K. N.; Strain, M. C.; Farkas, O.; Tomasi, J.; Barone, V.; Cossi, M.; Cammi, R.; Mennucci, B.; Pomelli, C.; Adamo, C.; Clifford, S.; Ochterski, J.; Petersson, G. A.; Ayala, P. Y.; Cui, Q.; Morokuma, K.; Malick, D. K.; Rabuck, A. D.; Raghavachari, K.; Foresman, J. B.; Cioslowski, J.; Ortiz, J. V.; Stefanov, B. B.; Liu, G.; Liashenko, A.; Piskorz, P.; Komaromi, I.; Gomperts, R.; Martin, R. L.; Fox, D. J.; Keith, T.; Al-Laham, M. A.; Peng, C. Y.; Nanayakkara, A.; Gonzalez, C.; Challacombe, M.; Gill, P. M. W.; Johnson, B.; Chen, W.; Wong, M. W.; Andres, J. L.; Gonzalez, C.; Head-Gordon, M.; Replogle, E. S.; Pople, J. A. *Gaussian 98*; Gaussian, Inc.: Pittsburgh, PA, 1998.

(18) Berti, P. J.; Schramm, V. L. *J. Am. Chem. Soc.* **1997**, *119*, 12069−12078.

**Chart 3**

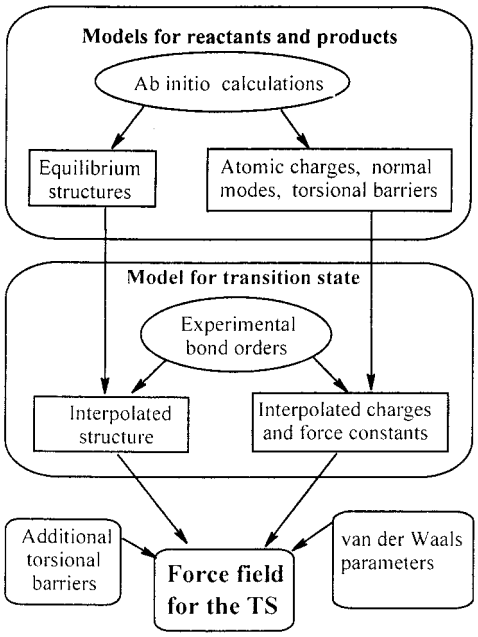


**Chart 4**

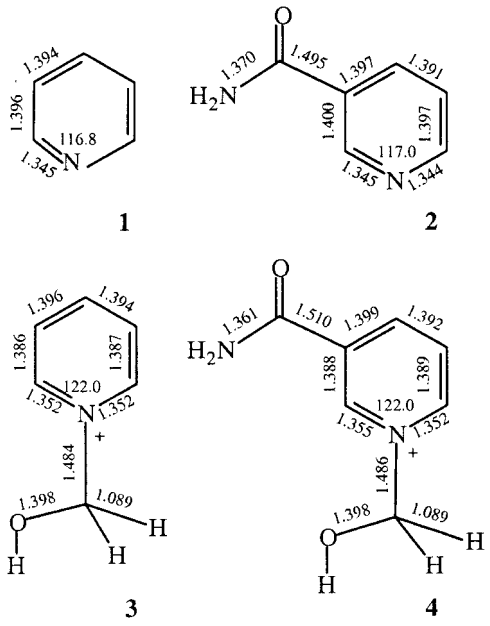


6-31+G(d,p) level. Models for ribo-oxocarbenium ions have been studied recently at the MP2/6-31+G(d) level.[19] We used several structural parameters from this study and also optimized carbenium ions **5**, **6**, and **7** (Chart 5) at the MP2/aug-cc-pVTZ levels to obtain more accurate estimates for carbon−oxygen bond lengths. These data along with the MP2/aug-cc-pVDZ structures of models **8** and **9** were used to estimate key structural parameters for ribo-oxocarbenium ion.

In the next stage, the CHARMM force field for model compounds was developed and tested by performing minimizations and torsional drivers for models **1**−**9**. The atomic charges for model compounds were obtained by fitting point charges to electrostatic potential derived from the MP2/aug-cc-pVDZ electron density using the CHelpG procedure.[20] The CHelpG charges for atoms in model compounds along with the charges used for E·NAD and E·TS simulation are listed in the Supporting Information. The Lennard-Jones parameters for oxocarbenium oxygen were refined by comparing the molecular mechanical and ab initio (BSSE-corrected MP2/aug-cc-pVDZ) interaction energy profiles for the oxocarbenium ion **5** and a water molecule. The bond force constants were derived by adjusting CHARMM force constants to reproduce the normal modes calculated at the MP2/aug-cc-pVDZ level for pyridine and oxocarbenium ions. The torsional parameters for ribo-oxocarbenium ion were derived based on a recently published ab initio conformational study of oxocarbenium ions.[19] In addition, the torsion barrier around the C2′−C1′ bond was determined at the MP2/aug-cc-pVDZ level for model **7**.

(19) Liang, G.; Sorensen, J. B.; Whitmire, D.; Bowen, J. P. *J. Comput. Chem.* **2000**, *21*, 329−339.

(20) Breneman, C. M.; Wiberg, K. B. *J. Comput. Chem.* **1990**, *11*, 361−373.

**Chart 5**

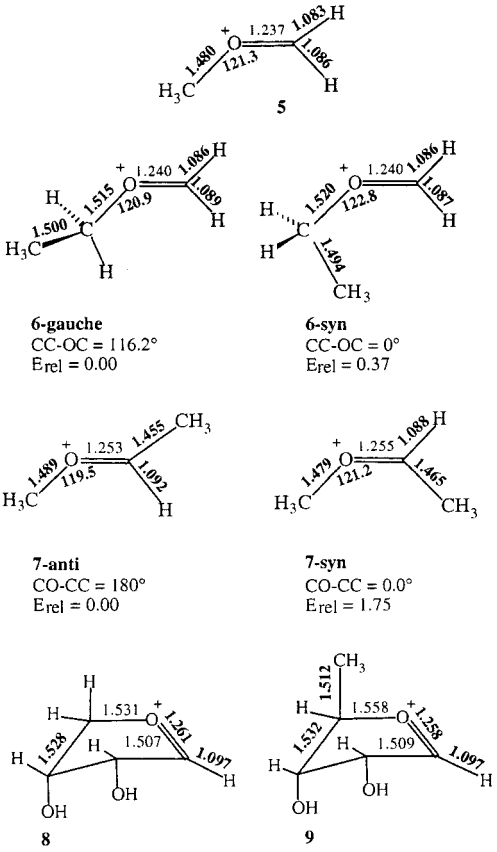


The structure of the nicotinamide portion of the TS was interpolated between 3-(aminocarbonyl)-1-hydroxymethyl pyridinium cation **4** and nicotinamide. The structure of the ribosyl cation in the TS was derived by interpolating between oxocarbenium ion models **5**−**9** and $NAD^+$ models **3** and **4**. The interpolation formulas have been reported previously.[18] The structure interpolation yields a model of transition state where the bond angles and dihedral angles around the N-ribosidic bond are undefined. The missing angle and dihedral values were assigned with the help of ab initio potential energy surface describing the bending and rotation around the N-ribosidic bond in the transition state. The surface was generated by performing a series of MP2/aug-cc-pVDZ single-point energy calculations for structures where bond angles and the dihedral $\chi$(O4′−C1′−N1′−C2) were assigned discreet values near the equilibrium geometry. The potential energy surface from MP2 calculations was used as a reference during the fitting of CHARMM force constants for bond bending and torsion terms involving the C1′−N1 bond. The bond stretching and bond bending force constants for the transition state are given in the Supporting Information. The interpolated TS structure (Chart 6) based on MP2 reference structures is similar to the previously proposed model.[7]

**Molecular Dynamics Simulations.** The hydrogen atoms were added to the X-ray coordinates of the catalytic subunit of diphtheria toxin and to the bound ligand with CHARMM. To assign the protonation state of ionizable groups, the environment around His21 was analyzed and it was concluded that the proton at Nϵ could form a hydrogen bond with the 2′-OH group of ligand ApUp. The assignment of this single histidine as HSP is also consistent with the experimental

**Chart 6**

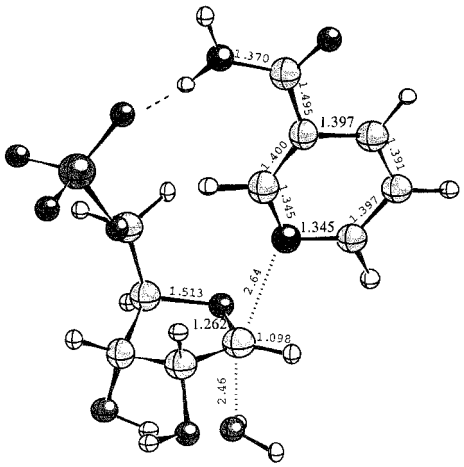


conditions for structure determination (pH 5.0 for the ApUp complex) and KIE measurements (pH 6.0).[7,14] The centered enzyme−ligand complexes (dimensions 56 × 46 × 36 Å) were solvated in a sphere of TIP3P water molecules[21] with radius 40.7 Å. If the oxygen of a water molecule was closer than 2.8 Å to any atom of the enzyme−ligand complex, the water molecule was deleted. The solvated systems were energy minimized and a stochastic boundary molecular dynamics simulation was initiated. Water molecules in the buffer region (spherical shell with thickness of 3 Å) were assigned a friction coefficient of 62 $ps^{-1}$ and followed Langevin equations of motion.[22] The reservoir region was represented by the soft boundary potential with a minimum at 41 Å.[23] All bonds containing hydrogens were constrained using the SHAKE algorithm.[24] Harmonic constraint of 50 kcal/mol $Å^2$ was applied, and gradually released, on protein backbone atoms to limit large conformational changes during the first 20 ps of heating. The system was heated slowly from 50 to 298 K by assigning velocities from Gaussian distribution. The total length of the simulations ranged from 1250 to 2000 ps. A time-step of 1.0 fs was used and the nonbonded interactions were updated every 20 steps. The nonbonded interactions were cut off at 12 Å by means of a force shifting function.

Trajectories of amino acids 1−186 after the first 360 ps were considered for analysis. Positional fluctuations around the average position were calculated for the backbone α-carbons and compared to those obtained from the crystal structure assuming that the latter were isotropic.[25] Positional fluctuations for bound ligands were calculated by overlapping the protein backbone atoms of sequential MD structures and averaging over all ligand atoms. The extent of intrinsic conformational freedom of ligands was assessed by performing least-squares overlap of all ligand atoms and calculating the fluctuations around the average structure. The extent of correlation between motions of backbone α-carbon atoms was calculated from the corresponding covariance matrix and plotted with the program GMT.[26]

## Results

**Structures of Model Compounds.** Ab initio optimizations yield two conformers for nicotinamide which differ in the orientation of the carboxamide oxygen relative to the C4 atom (Figure 1, top). The trans conformation with $\kappa$(O7−C7−C3−C2) = 147° is the global minimum in the gas phase. The MP2/aug-cc-pVDZ//MP2/6-31+G(d,p) calculations predict that the cis conformation with $\kappa$ = 36° lies 0.77 kcal/mol above the trans conformation. This result is consistent with the recent crystal structure determination of nicotinamide.[27] Rotation of the carboxamide arm in nicotinamide faces a barrier of 2.77 kcal/mol and interconversion of rotamers is expected to be rapid in vacuo. The trans preference in the neutral nicotinamide contrasts with the orientation of the carboxamide arm on N-substituted pyridinium compounds.[28] We found that 3-(aminocarbonyl)-1-hydroxymethyl pyridinium cation **4** has six energy minima at the MP2/6-31+G(d,p) level (Figure 1). Those minima can be classified based on torsion angles $\kappa$ and $\chi$, corresponding to the orientation of the carboxamide oxygen relative to C2 (cis−trans), and the hydroxymethyl group (syn−anti), respectively. The global minimum for model **4** has the carboxamide arm in the cis orientation and the *N*-hydroxymethyl group is in the anti conformation. Local minima with the carboxamide arm in the trans orientation lie 1−2 kcal/mol above the global minimum.

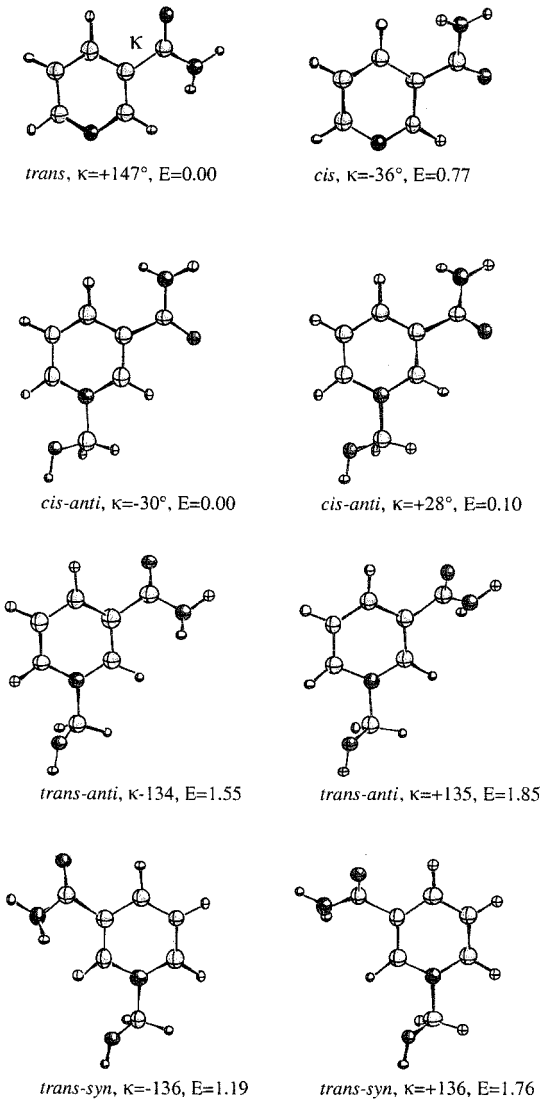


**Figure 1.** Conformers of nicotinamide and 3-(aminocarbonyl)-1-hydroxymethyl pyridinium cation at the MP2/6-31+G(d,p) level. Relative energies are calculated at the MP2/aug-cc+pVDZ level. See the Supporting Information for selected XYZ coordinates and absolute energies.

(21) Jorgensen, W. L.; Chandrasekhar, J.; Madura, J. D.; Impey, R. W.; Klein, M. L. *J. Chem. Phys.* **1983**, *79*, 926−935.
(22) Brooks, C. L., III; Karplus, M. *J. Mol. Biol.* **1989**, *208*, 159−181.
(23) Brooks, C. L., III; Brünger, A.; Karplus, M. *Biopolymers* **1985**, *24*, 843−865.
(24) Ryckaert, J. P.; Ciccotti, G.; Berendsen, H. J. C. *J. Comput. Phys.* **1977**, *23*, 327−341.
(25) McCammon, J. A.; Harvey, S. *Dynamics of proteins and nucleic acids*; Cambridge University Press: Cambridge, 1987; Chapter 5.
(26) Wessel, P.; Smith, W. H. F. *EOS Trans. AGU* **1998**, *79*, 579.
(27) Miwa, Y.; Mizuno, T.; Tsuchida, K.; Taga, T.; Iwata, Y. *Acta Crystallogr., Sect. B: Struct. Sci.* **1999**, *B55*, 78−84.
(28) De Luca, G.; Marino, T.; Mineva, T.; Russo, N.; Toscano, M. *J. Mol. Struct. (THEOCHEM)* **2000**, *501−502*, 215−220.

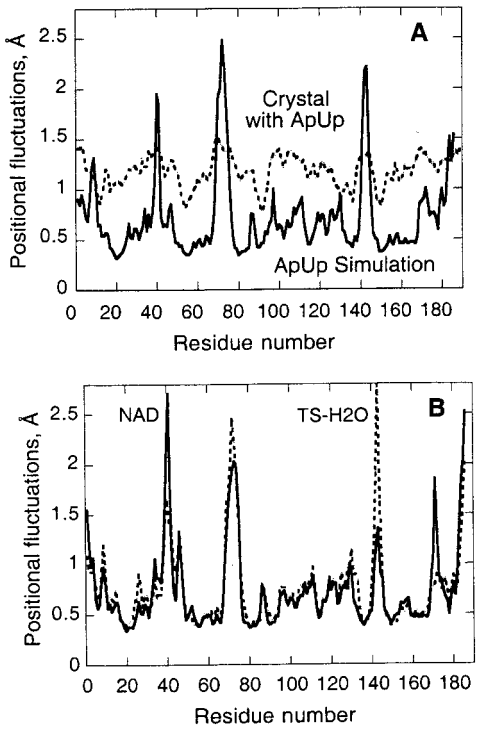


**Figure 2.** Positional fluctiations for α-carbons in the E·ApUp complex during the simulation and in the crystal structure (panel A) and comparison of positional fluctuations for α-carbons from the E·S and E·TS simulations (panel B).

The oxocarbenium ion **6** has two stable conformations corresponding to the rotation around the C−C−O$^+$=C dihedral. The minimum energy conformation occurs when this dihedral angle is 116.2°; the second stable conformer has C−C−O$^+$=C at 0° and is 0.37 kcal/mol above the ground state at the MP2/aug-cc-pVTZ level. We note that the shape of the torsional barrier for this molecule at the MP2/aug-cc-pVTZ level is significantly different than the recently reported MP2/6-31+G(d) profile and suggest a revision of the corresponding MM3 parameter.[19] The barrier for rotation around the H−C−O$^+$=C bond in model **5** is 1.09 kcal/mol, somewhat higher than the MP2/6-31+G(d,p) value 0.77 kcal/mol. Model **7** has two minima, the syn conformation with C−O$^+$=C−C at 0° is 1.75 kcal/mol above the anti structure. The barrier for rotation around the C−C bond in model **7** was 0.57 kcal/mol.

**Molecular Dynamics Simulations.** The molecular dynamics simulations of solvated E·I, E·S, E·TS, and E·TS−$H_2O$ produced stable trajectories after the initial heating and equilibration period (figure included in the Supporting Information). The calculated root-mean-square deviation of the backbone atoms $C_\alpha$, C, N, and O differed on average by 1.5 Å from the crystal structure of E·I during the production period. The overall structure of the protein backbone did not change significantly from the crystal structure with the exception of the C-terminal α-helix. For this helix, differences from the initial structure include unfolding of four last residues and the overall change in orientation by about 30° relative to the rest of the protein. Positional root-mean-square fluctuations of α-carbons from the E·I simulation show five regions of high flexibility (Figure 2A). Four of these regions correspond to loops in the protein structure while the last region includes the C-terminal α-helix. The comparison of positional fluctuations from our MD simulations and those obtained from experimental Debye−Waller B-factors for the crystal structure of E·I (Figure 2A) show that regions with high flexibility during the simulation are also flexible in this crystal structure. However, many residues that were rigid during the dynamics had large experimental temperature factors. This discrepancy could be due to the presence of alternative conformations which interconvert slower than the time scale of simulation, and thus may reflect insufficient sampling. However, since the protein structure in these regions was very similar to the crystal structure throughout the simulation, it is more likely that the discrepancy arises from the static lattice disorder in protein crystals.[25] The backbone positional fluctuations from E·S, E·TS, and E·TS−$H_2O$ simulations are similar to the E·I results (Figure 2B).

Analysis of the correlation of atomic motions revealed that several residues moved in a concerted manner (for correlation plots of α-carbon atoms see Supporting Information). Most significant positive correlations were observed in secondary structure elements such as $\beta$-sheets (Figure 3). These positive correlations were quite similar in the E·S, E·I, and E·TS−$H_2O$ simulations. The pattern of anticorrelated motions was also similar between the E·S and E·I simulation, but the E·TS−$H_2O$ simulation produced a different pattern of correlated motions. The most prominent anticorrelation was present between the active site loop and a distal loop, which form the two "walls" of the active site, when $NAD^+$ was bound. The motion of backbone atoms of residues 48−54 in the so-called "active site loop" was anticorrelated with the motion of atoms in the loop at the bottom of the active site (residues 72−74, labeled with stars in Figure 4). The distance between these residues is over 25 Å. Interestingly, this anticorrelation was nearly absent in the E·TS−$H_2O$ simulation.

The conformation of the bound inhibitor ApUp is somewhat different from that of the bound $NAD^+$ since it has only one phosphate ester moiety linking the two nucleosides (Chart 1). Despite structural differences, the inhibitor and substrate fit to the active site in a similar way (compare with Chart 2). The overall shape of the bound ApUp remained virtually unchanged throughout the 2 ns dynamics. The only conformational transition observed involved the rotation of the hydroxymethyl group around the C4′−C5′ bond in the adenosyl part of the inhibitor. During the first part of the simulation the hydrogen at the O5′ was hydrogen bonded to the O2′ of the ribose adjacent to uracil. This interaction broke after 1.25 ns and a new hydrogen bond between the O5′ hydrogen and N3 of adenine formed shortly thereafter. The uracil base remained in the *−anticlinal* orientation, and the adenine base was in the *synclinal* orientation throughout the simulation. The structure of ApUp throughout the simulation differed by 0.75 Å from the X-ray crystal structure, and the fluctuations in movement were 0.17 Å on average after the least-squares fit of the inhibitor atoms. The average of positional fluctuations of ApUp increased to 0.61 Å when coordinates of protein backbone atoms were used for overlapping sequential MD structures, indicating that the bound inhibitor has limited translational and rotational freedom in the active site.

The freedom of motion in bound substrate $NAD^+$ was considerably larger than that with ApUp and several distinct conformers were observed during the 1.91 ns MD simulation (Figure 4). The initial structure of $NAD^+$ is characterized by the C3′-*endo* pucker of the ribose in the nicotinamide mononucleotide moiety, *synclinal* orientation of the adenine base, and C2′-*endo* pucker of the adenosyl 3′-mononucleotide. During the equilibration period, the ribose ring in the nicotinamide mononucleotide moiety adopted a C2′-*endo*−C3′-*exo* twist conformation that persisted throughout the simulation (pseudorotation phase angle[31] 180 ± 12°). The nicotinamide moiety remained

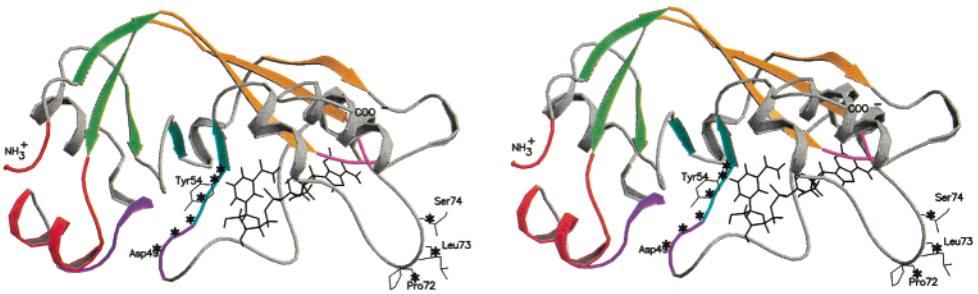


**Figure 3.** Mapping of the correlated motions to the structure of the diphtheria toxin catalytic subunit complexed with $NAD^+$. If two residues show a positive correlated motion they are colored with the same color, i.e. the motion of the aminoterminal coil is correlated with the motion of a nearby α-helix (red). Residues which do not show significant positive correlated motions are displayed in gray. The residues in two segments which display strong anticorrelated motions in the E·S are designated by stars. This stereoplot was generated with programs MOLSCRIPT[29] and Raster3D.[30]

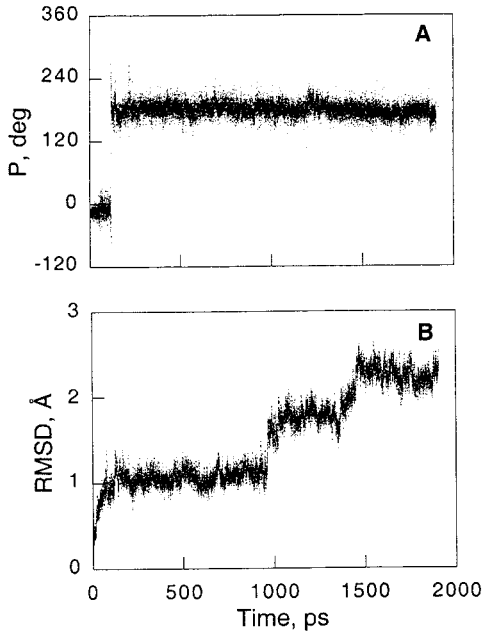


**Figure 4.** Changes in NAD+$^+$ conformation during the E·S simulation. The top panel shows the pseudorotation angle for the ribose ring; the bottom panel displays the root-mean-square deviation from the initial structure.

in the syn orientation ($\chi_{Nic} = 17 \pm 10°$) but the adenine ring underwent a transition from +*synclinal* ($\chi_{Ade} = 71 \pm 11°$) to anti conformation ($\chi_{Ade} = 180 \pm 20°$) at 965 ps. This conformational change was accompanied with a loss of two hydrogen bonds between adenine and the enzyme. The carboxamide arm of nicotinamide remained in the trans conformation throughout the simulations and was hydrogen bonded to the peptide group of Gly22. Comparing the mobilities within the 360−965 ps time range indicates that the bound $NAD^+$ has more freedom of movement than ApUp (average of positional fluctuations 0.67 Å vs 0.56 Å, respectively). Nicotinamide stayed in the syn orientation and adenine remained in the +*synclinal* orientation throughout the E·TS and E·TS−$H_2O$ simulations.

The main interactions of the substrate or the transition state with enzymatic residues are depicted in Chart 2 and Figure 5. The carboxylate of Glu148 is the nearest charged group to the reaction center. This group was distant from the bound ligand when the active site is occupied by ApUp. The distance between the nearest carboxylate oxygen of Glu148 and C1′ of Up was more than 7 Å during the E·I simulation. The carboxylate group was significantly closer when $NAD^+$ was bound in the active site, with an average distance of 4.5 ± 0.5 Å between the nearest oxygen and C1′. Interestingly, a hydrogen bond between the carboxylate oxygen and the 2′-OH hydrogen was present in 17% of E·S structures and in 57% of E·TS−$H_2O$ structures (Figure 6). Taken alone this information would suggest Glu148 to be involved in catalysis. Different behavior was observed for Asn45 that also was interacting with the ribose ring of $NAD^+$. The side-chain carbonyl oxygen of Asn45 formed hydrogen bonds to the ribose 2′-OH (12% of the time) and 3′-OH (33% of the time). Somewhat surprisingly, hydrogen bonds from Asp45 were virtually absent in the E·TS−$H_2O$ simulation. It would be interesting to analyze catalytic properties of mutant enzymes where Asn45 has been replaced.

Another catalytically important region in diphtheria toxin involves residues 34−52 which form an extended loop, called an "active-site" loop.[6] The residues of this loop make extensive contact with the bound ligands (Charts 1 and 2). However, these interactions are not near the nicotinamide or the scissile bond with the exception of Asn45. The active-site loop is well ordered in the crystal structures of the free enzyme and E·I but this region is disordered in the E·S complex. The same conclusion emerges from the comparison of positional fluctuations from the simulations. The active site loop is most flexible in the E·S complex followed by the E·I and E·TS. Residues Gly34 and Gln36 in the active site loop make hydrogen bonds to the adenine of $NAD^+$ in available crystal structures. These interactions were observed throughout the E·I, E·TS, and E·TS−$H_2O$ simulations as well as in the E·S complex before 965 ps. Interestingly, these two hydrogen bonds break in the E·S simulation at 965 ps and do not form thereafter (Figures 7 and 8). This loss of hydrogen bonding may correspond to early steps for dissociation of $NAD^+$ from the enzyme, or it may represent an alternative conformation for the bound $NAD^+$. The latter possibility is supported by the experimental observation that 8-$N_3$-NAD photolabels an unidentified amino acid within the segment Ser40-Phe53.[32] We find that in this alternative conformation the C8 of Ade is rotated toward Phe53 and the closest carbon atoms of the aromatic side-chain are within 6.5 Å from the C8 carbon of the adenine moiety. We suggest that the labeled residue is Phe53 and not Trp50, which is more than 10 Å from the C8 carbon of adenine throughout the MD simulation. Further experimental work to identify the site of photolabeling is needed to resolve this question.

(29) Kraulis, P. J. *J. Appl. Crystallogr.* **1991**, *24*, 946−950.
(30) Merritt, E. A.; Bacon, D. J. *Methods Enzymol.* **1997**, *277*, 505−524.
(31) Johnson, R. W.; Marschner, T. M.; Oppenheimer, N. J. *J. Am. Chem. Soc.* **1988**, *110*, 2257−2263.
(32) Lodaya, R.; Blanke, S. R.; Collier, R. J.; Slama, J. T. *Biochemistry* **1999**, *38*, 13877−13886.

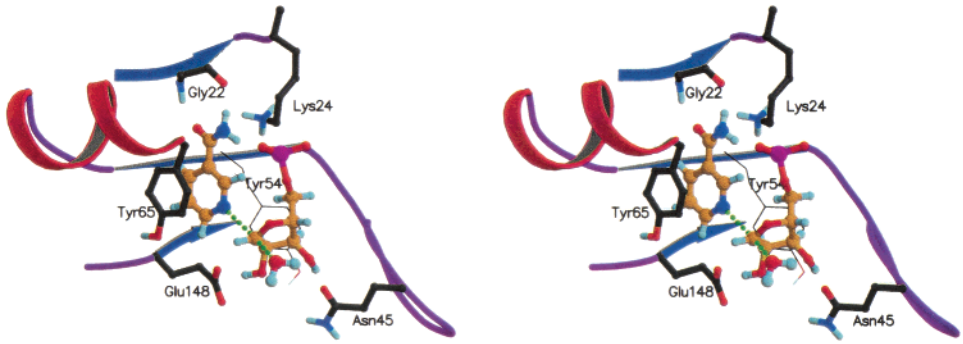


**Figure 5.** Stereoplot showing the position of enzymatic residues near the scissile bond of $NAD^+$. The aromatic side-chain of Tyr65 stacks on top of the nicotinamide ring similarly in E·S, E·TS-$H_2O$, and E·I. The figure was generated with programs MOLSCRIPT[29] and Raster3D[30].

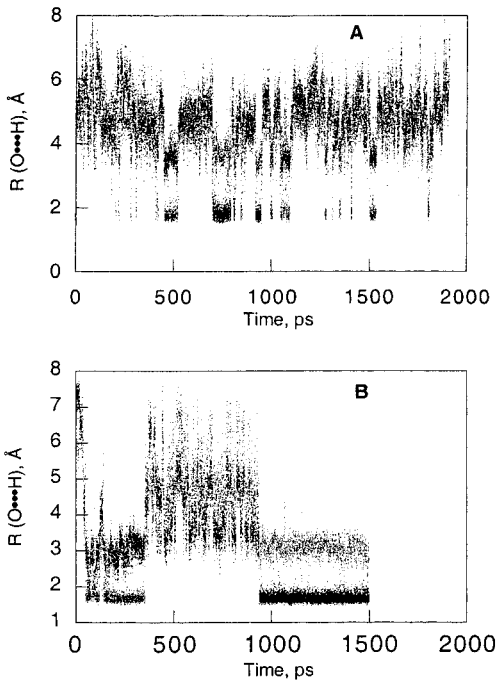


**Figure 6.** Formation and breaking of the hydrogen bond between the active site Glu148 and the ribose 2′-OH of the bound ligand during the E·S (panel **A**) and E·TS (panel **B**) simulation.

## Discussion

Spontaneous hydrolysis of $NAD^+$ is a slow process at neutral pH. Below pH 7, the reaction is pH independent and proceeds by direct attack of a water molecule on $NAD^+$ with a first-order rate constant of $5 \times 10^{-7}$ $s^{-1}$.[31] From the temperature dependence of the rate constant, an activation enthalpy of 25.2 kcal/mol can be estimated. At pH values above p$K_a$ = 11.7, the species which hydrolyzes is the anion of $NAD^+$ where one of the protons from ribose hydroxyls has dissociated. The rate constant for the hydrolysis of the anion is 10 000 times greater than that of the parent $NAD^+$.[31] The enzymatic hydrolysis is characterized by a pH-independent second-order rate constant $k_{cat}/K_m$ of 10.9 $M^{-1}$ $s^{-1}$.[7] In this reaction, product release is not rate limiting, and $k_{cat}$ ($3 \times 10^{-3}$ $s^{-1}$) reflects the rate of the chemical step. Also, there appears to be no external commitment and the $K_m$ is close to the dissociation constant $K_s^{NAD}$. At maximal velocity, diphtheria toxin accelerates the hydrolysis of $NAD^+$ nearly 6000-fold. Thus, ionization of the ribose 2′-OH provides a greater increase in $NAD^+$ hydrolysis than does enzymatic catalysis. Oppenheimer et al. suggested that making a hydrogen bond to the 2′-OH hydrogen would have a catalytic effect as the 2′-oxygen develops a partial negative charge.[33] This partial negative charge helps to stabilize the formation of an oxocarbenium ion. Based on experimental evidence that Glu148 is near the scissile glycosyl bond,[11,34,35] this residue was proposed to function as a hydrogen bond acceptor from the ribose 2′-hydroxyl group.[33] However, the X-ray structure with bound $NAD^+$ did not support this view as the distance from Glu148 carboxylate oxygens to the 2′-OH oxygen was 3.4 Å. Since the carboxylate group was within 4 Å of the C1′ of ribose as well as of the N1 of nicotinamide, a direct electrostatic stabilization of the ribo-oxocarbenium ion-like transition state was proposed instead.[5] However, it was subsequently pointed out that an electrostatic interaction of Glu148 with the nicotinamide ring in the ground state would result in an "anticatalytic" effect.[7] In our E·S simulation the carboxylate group stayed within 4.5 Å of the C1′ and N1 atoms throughout the E·S simulation. Similar distances are observed in both transition state simulations. Thus, the MD results are not consistent with either a anticatalytic effect or the direct electrostatic TS stabilization mechanism. Instead, simulations of the E·S complex show that the 2′-OH hydrogen makes a hydrogen bond to Glu148 about 17% of the time ($R_{H\cdots O} = 1.95 \pm 0.10$ Å) but stays between 4 and 6 Å for the rest of the time (Figure 6). In E·TS this hydrogen bond is present 57% of the time. Thus, current MD simulation reveales a dynamic equilibrium between the hydrogen bonded and noninteracting states which was masked in the time-average crystal structure. This hydrogen bonding should result in charge relocalization in both ground and transition states facilitating formation of a oxocarbenium ion-like TS. However, experimental mutagenesis studies suggest that Glu148 is not necessary for $NAD^+$ hydrolysis since replacement of Glu148 with aspartate or glutamine does not affect the $k_{cat}$ for the enzymatic hydrolase reaction.[11] Glu148, however, provides (100−300)-fold rate acceleration in the ADP−ribosyltransferase reaction.[11] By assuming that the persistent hydrogen bonding to the carboxylate group gives at most 10% rate acceleration compared to the fully dissociated diol anion, and noting that such bonding was observed 17% of the time in E·S simulation, rate acceleration due to the Glu148···2′OH interaction would be no more than 170-fold. Such an estimate is consistent with observed NAD−ribosyltransferase activities of mutants. Studies are underway in our laboratory to generate the computer models of the cited mutant enzymes.

Another proposed role for Glu148 involves the activation of the incoming nucleophile. It was suggested that Glu148 may

(33) Oppenheimer, N. J. *Mol. Cell. Biochem.* **1994**, *138*, 245−251.
(34) Carroll, S. F.; Collier, R. J. *Proc. Natl. Acad. Sci. U.S.A.* **1984**, *81*, 3307−3311.
(35) Carroll, S. F.; McCloskey, J. A.; Crain, P. F.; Oppenheimer, N. J.; Marschner, T. M.; Collier, R. J. *Proc. Natl. Acad. Sci. U.S.A.* **1985**, *82*, 7237−7241.

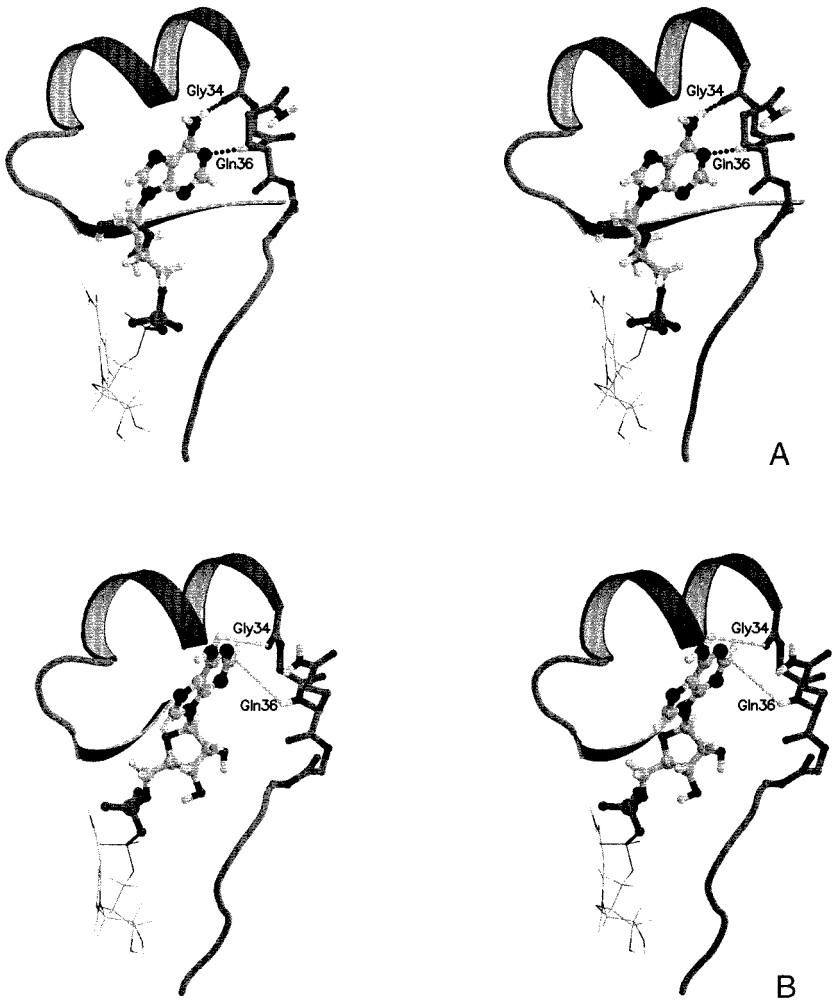


**Figure 7.** Comparison of the conformation and hydrogen bonding interactions in the adenine moiety of $NAD^+$ at 950 (A) and 1910 ps (B). The active site loop starts at position Gly34. This stereoplot was generated with programs MOLSCRIPT[29] and Raster3D[30].

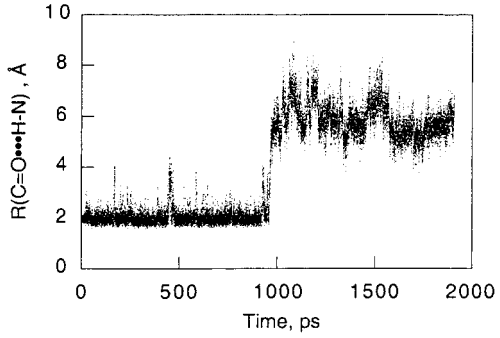


**Figure 8.** Formation and hydrogen bond between the $NH_2$ hydrogen of the adenine moiety of $NAD^+$ and the backbone carbonyl of Gly34 in the E·S simulation. The profile for Gln36−Ade interaction follows a similar time-course.

function by polarizing the H−O bond of water to promote nucleophilic attack.[7] Our simulations do not support the latter hypothesis—the carboxylate group does not reach the underside of the ribose ring of the nicotinamide moiety which is exposed to the solvent. The finding warrants reconsideration of the Glu148 carboxylate's role in the ADP−ribosylation reaction where it is thought to activate the diphthamide imidazole for a nucleophilic attack.[11] It appears that a significant structural change of the active site is required for such activation.

Another residue that has been implicated in diphtheria toxin catalysis is His21 (Chart 2). The pH studies suggest that this single conserved histidine titrates with a kinetically observable p$K_a$ of 6.3, and protonation of this group is required for the enzymatic activity.[8,11] Mutation of this residue abolishes $NAD^+$ binding and reduces $k_{cat}$ for the hydrolytic reaction.[9] Structural studies have shown that this residue hydrogen bonds to the backbone carbonyl of Tyr54 as well as to the 2′-oxygen of the ribosyl moiety of ADP. These interactions were also seen in the current simulation. The hydrogen at N$\delta$ of His21 formes a persistent hydrogen bond with the backbone carbonyl of Tyr54 in all four simulations. The second hydrogen at N$\epsilon$ of His21 hydrogen bonded to the 2′ oxygen throughout the E·I simulation but was interacting with the phosphate group of adenine in E·TS and E·TS−$H_2O$ simulations. In the beginning of the E·S simulation this hydrogen was interacting with the 2′ oxygen but this interaction broke around 950 ps and a hydrogen bond to phosphate oxygens formed shortly thereafter. The results support a model where protonated His21 is required for $NAD^+$ binding through interaction with either the ribose or phosphate moiety of ADP. Its previously proposed role, hydrogen bonding to the carboxamide arm of nicotinamide,[9] is not supported. The backbone atoms of adjacent Gly22 anchor the carboxamide arm instead.

Several aromatic amino acids are implicated in binding and hydrolysis of $NAD^+$. Tyr65 is in face-to-face contact with the nicotinamide moiety (Figure 5). This interaction is observed throughout all the simulations and was also present in crystal structures with ligated DT. The distance between the two rings

in the E·S and E·TS−$H_2O$ simulations are identical (both 3.88 ± 0.24 Å), suggesting that stacking with Tyr65 does not stabilize the transition state over the ground state. This notion is well supported by mutagenesis studies which show that while the Tyr65Ala mutant has greatly reduced binding affinity toward $NAD^+$, the $k_{cat}$ for the $NAD^+$ hydrolysis is higher in the alanine mutant compared to the wild-type enzyme.[10] Our results are consistent with the hypothesis that the interaction with Tyr65 serves to position the leaving group in a orientation where EF2 can approach the substrate from a favorable angle.[10] A second tyrosine residue in the active site, Tyr54, does not stack with the nicotinamide but seems to be required to maintain the active site structure.

Ground-state destabilization has been invoked to explain accelerated $NAD^+$ hydrolysis by diphtheria toxin. For example, the syn conformation of the nicotinamide ring places O4′ and C2 of the nicotinamide mononucleotide moiety in an eclipsed conformation. The resulting steric overlap was predicted to destabilize the ground state and makes the nicotinamide a better leaving group.[36] The average distance between the O4′ and H2 of the nicotinamide is 2.34 ± 0.10 Å from the E·S simulation. These atoms are 2.40 Å apart in the most stable gas-phase conformer, suggesting that similar steric strain also contributes to the lowering of the activation barrier in the spontaneous reaction. So, even though this steric effect destabilizes the ground state, it does not contribute significantly to the difference between enzymatic and spontaneous reaction rates. However, current calculations reveal another possible effect that can lower the activation energy specifically in the enzymatic reaction.

Ab initio calculations indicate that the carboxamide arm in unbound N-substituted nicotinamides, such as $NAD^+$, prefers a cis orientation.[16,28,37−40] However, a neutral nicotinamide molecule prefers a trans orientation. The nonenzymatic hydrolysis of $NAD^+$ most likely involves substrate with the carboxamide arm in the cis-anti orientation which yields *cis*-nicotinamide in the rate limiting step; the product converts subsequently to *trans*-nicotinamide. The enzyme-catalyzed reaction, however, starts with the substrate in the higher energy trans-syn conformation, but yields product in its global minimum. Since the transition state for this reaction is very product-like, the activation energy difference between spontaneous and catalyzed reactions is close to the difference in reaction enthalpies. The latter can be calculated from ab initio energies of reactants and products, and is 1.96 kcal/mol. The enzyme lowers the activation energy by ∼2 kcal/mol compared to the spontaneous reaction by virtue of binding the substrate carboxamide arm in a high-energy conformation. This would lead to 27 times rate acceleration assuming equal Arrhenius prefactors for spontaneous and catalyzed reactions.

Computer simulation techniques can reveal any role of motions in creating reactive conformations (NACs)[41,42] and could uncover protein motions that couple with the reaction coordinate.[43] While coupling of local enzyme motions to substrate motions is relatively well understood, the putative role of long-range couplings to catalysis is not clear.[42] Such motions are expected to manifest as correlated or anticorrelated motions of protein atoms and can be readily identified by examining the elements of the cross-correlation matrix. The covariance analysis of fluctuations in the diphtheria toxin catalytic subunit reveals that most positive correlations occur between residues which are either part of the common secondary structure element or make significant interchain contacts at the tertiary structure level (Figure 3). Comparison of positive correlated motions from E·S, E·TS−$H_2O$, and E·I simulation did not reveal any motions unique to the E·S complex. Interestingly, a unique anticorrelated motion between the active site loop and the distal loop, which are about 20−25 Å apart, was found when negative matrix elements were plotted. Despite the fact that this anticorrelated motion occurs near the reaction site, it remains unclear how it could affect the catalysis of $NAD^+$ hydrolysis. It should be noted that pronounced correlated motions unique to the E·S complex have been observed previously in the study of dihydrofolate reductase.[44]

## Conclusions

We have used ab initio calculations and molecular dynamics simulations to evaluate concepts as to, how diphtheria toxin can achieve the observed 6000-fold rate acceleration ($\Delta\Delta G^{\ddagger} \sim 5$ kcal/mol) for $NAD^+$ hydrolysis compared to the noncatalyzed reaction in water. Among the factors considered in our analysis are the following: (i) binding of the nicotinamide portion of the substrate in a high-energy conformation, (ii) charge relocalization from the ribose ring through a hydrogen bond to Glu148, and (iii) freedom of motions in the ground state and transition state. The carboxamide arm of the leaving group prefers a cis orientation in the free $NAD^+$, but the substrate is bound to the enzyme in the trans orientation. Since the product prefers the trans conformation for the carboxamide arm, this leads to an overall 2 kcal/mol reduction of the activation barrier compared to the noncatalyzed reaction. Molecular dynamics simulations revealed that the active site residue Glu148 hydrogen bonds to the 2′-hydroxyl hydrogen of ribose ∼20% of the time in the ground state and nearly 60% of the time in the transition state. The increase in negative charge at the 2′-oxygen would be expected to facilitate the formation of the oxocarbenium ion-like TS. Since it is well established that the ionization of the 2′-hydroxyl group of $NAD^+$ accelerates the nonenzymatic hydrolysis 10 000-fold, it is hard to conceive that the enzyme does not utilize such a mechanism. Mutagenesis experiments, however, have shown that glutamine or aspartate residues replace Glu148 without loss of hydrolytic activity.[11] Last, comparison of thermal fluctuations from MD simulations indicates that the substrate retains more freedom in the active site than the inhibitor. The bound substrate and the transition state had a comparable freedom of motion up to 965 ps. However, the difference in binding interactions after 965 ps is distant from the reaction center. This difference in thermal fluctuations cannot be easily linked to a value of $\Delta G^{\ddagger}$ as the ligand mobility affects binding enthalpies and entropies in the opposite direction. It is likely that all the above-discussed effects do play roles also in the enzymatic NAD−ribosyltransferase reaction.

**Acknowledgment.** This research was funded by the National Science Foundation grant MCB-9727937. The authors thank Professors Paul Berti and Vern Schramm for helpful discussions

(36) Bell, C. E.; Eisenberg, D. *Adv. Exp. Med. Biol.* **1997**, *419*, 35−43.
(37) Almarsson, Ö.; Bruice, T. C. *J. Am. Chem. Soc.* **1993**, *115*, 2125−2138.
(38) Oppenheimer, N. J.; Handlon, A. L. *Mechanism of NAD-dependent enzymes*; Academic Press: New York, 1992; Vol. 20, pp 454−505.
(39) Wu, Y. D.; Houk, K. N. *J. Am. Chem. Soc.* **1991**, *113*, 2353−2358.
(40) Schiøtt, B.; Zheng, Y.-J.; Bruice, T. C. *J. Am. Chem. Soc.* **1998**, *120*, 7192−7200.
(41) Bruice, T. C.; Lightstone, F. C. *Acc. Chem. Res.* **1999**, *32*, 127−136.
(42) Bruice, T. C.; Benkovic, S. J. *Biochemistry* **2000**, *39*, 6267−6274.
(43) Lau, E. Y.; Bruice, T. C. *J. Am. Chem. Soc.* **1998**, *120*, 12387−12394.
(44) Radkiewicz, J. L.; Brooks, C. L., III. *J. Am. Chem. Soc.* **2000**, *122*, 225−231.

and for providing the partial structure of the experimental transition state. The authors are grateful for computer time on UCSB's Origin2000 which is partially funded by grants from the National Science Foundation (CDA96-01954) and Silicon Graphics Inc.

**Supporting Information Available:** Residue topology description and force constants for the transition state and ab initio structures for conformers of nicotinamide and 3-(aminocarbonyl)-1-hydroxymethyl pyridinium cation as well as figures illustrating root-mean-square deviation of protein backbone atoms and correlation of α-carbon motions (PDF). This material is available free of charge via the Internet at http://pubs.acs.org.

JA0113807